Theses and Dissertations

Theses, Dissertations, and Senior Projects

January 2018

Synthesis And Characterization Of Novel Metal-Ti3sic2 Based Multilayered Composites

Quan Tien Tran

Follow this and additional works at: https://commons.und.edu/theses

SYNTHESIS AND CHARACTERIZATION OF NOVEL METAL-Ti$_3$SiC$_2$ BASED MULTILAYERED COMPOSITES

by

Quan Tien Tran

Bachelor of Science, University of North Dakota, 2016

A Thesis

Submitted to the Graduate Facility

of the

University of North Dakota

In partial fulfillment of the requirements
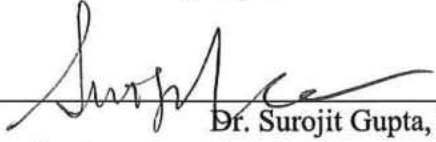
For the degree of

Master of Science

Grand Forks, North Dakota

December

2018

This thesis, submitted by Quan Tien Tran in partial fulfillment of the requirements for the Degree of Master of Science from the University of North Dakota, has been read by the Faculty Advisory Committee under whom the work has been done and is hereby approved.

_____
Dr. Surojit Gupta, Ph.D.

_____
Dr. Clement Tang, Ph.D.

_____
Dr. Cai Xia Yang, Ph.D.

This thesis meets the standards for appearance, conforms to the style and format requirements of the School of Graduate Studies at the University of North Dakota, and is hereby approved.

_____
Grant McGimpsey
Dean of the School of Graduate Studies

_____
December 6, 2018
Date

iii

PERMISSION

Title   Synthesis and Characterization of Novel Metal-Ti_3SiC_2 Based Multilayered Composites

Department   Mechanical Engineering

Degree   Master of Science

In presenting this thesis in fulfillment of the requirements for a graduate degree from the University of North Dakota, I agree that the library of this University shall make it freely available for inspection. I further agree that permission for extensive copying for scholarly purposes may be granted by the professor who supervised my thesis work or, in his absence, by the chairperson of the department or the dean of the School of Graduate Studies. It is understood that any copying or publication or other use of this thesis or part thereof for financial gain shall not be allowed without my written permission. It is also understood that due recognition shall be given to me and to the University of North Dakota in any scholarly use which may be made of any material in my thesis.

Signature   Quan Tien Tran

Date   6 Dec 2018

TABLE OF CONTENTS

LIST OF FIGURES

LIST OF TABLES

ACKNOWLEDGEMENTS

I would like to dedicate this work to my mother, Mrs. Duoc Nguyen, whose dreams for me have resulted in this achievement and without her loving upbringing and nurturing, I would not have been where I am today and what I am today. Thank you for your dedication and sacrificed that you made for your sons and your grandchildren.

ABSTRACT

In this thesis, the design and development of novel multilayered MAX reinforced metal (MRMs) composites is reported. In literature, different studies have focused on MAX Reinforced Metals (MRMs) composites, however no research on MRMs have been on multilayered composites. In this thesis, two different types of composites were designed, (a) Type I, and (b) Type II multilayered composites. In type I composites, MRMs layers were interleaved between metal layers to create a multilayered composite. Similarly, in Type II composites - MRMs were interleaved with two different types of metal layers. In the Chapter II, synthesis of the Ni-Ti$_3$SiC$_2$ multilayered Type I and II composites, and their mechanical and tribological behavior have been reported. In Chapter III, a commercial AlSi alloy was substituted with pure Ni as the metal matrix to design Type I composites. The detailed microstructure, mechanical, and tribological behavior will be reported in this thesis.

CHAPTER I
INTRODUCTION

1.1 Lubrication

When human first invented the wheel, we probably used lubricants to prevent wears and tears. Earlier lubrication including animal fat, animal oil, and vegetable oils, has been practiced for millennia. With the discovery of petroleum, the use of inexpensive oils as lubrication had rapidly expended. A lubricant is any substance that reduces friction and wear, provides smooth running, and a satisfactory life for machine elements. Most lubricants are liquids (such as mineral oils, synthetic esters, silicone fluids, and water), they may be solids (such as polytetrafluoroethylene, or PTFE) for use in dry bearings, greases for use in rolling-element bearings, or gasses (such as air) for use in gas bearings [1]. Since the mid 1930's, a strong trend has developed toward using higher temperature in moving parts. As temperature increases, the viscosity of the fluid significantly drops, and conversely as temperature decreases, the viscosity significantly increases. Furthermore, the relationship between fluid lubricants and pressure is also a crucial component of fluid lubrication. Increases in pressure will result in increases in viscosity and the lubricant may lose some of its liquid properties and behave more like a wax [2, 3]. But if the pressure drops below the fluid vapor pressure, the fluid will unstably rupture and instantaneously cavitate [3, 4]. Since the petroleum oils could not adequately do the job at high temperatures, new synthetic lubricant materials were introduced. Temperatures now encountered in supersonic aircraft, spacecraft, and certain industrial applications are beyond the useful range of even the synthetic lubricant. One result of this trends has been the development and usage of solid lubricants to obtain the necessary lubrication of delicate parts at extreme temperature and pressures [5].

In most tribological applications, liquid or grease lubricants are used to combat friction and wear; but when service conditions become very severe (i.e., very high or low temperatures, vacuum, radiation, extreme contact pressure, etc.), solid lubricants may be the only choice for controlling friction and wear [6]. A solid lubricant is a material used as powder or thin film which reduces friction and wear of contacting surfaces in relative motion and provides protection from damage. Solid lubricant friction is a special form of friction which occurs when using solid lubricants. It differs from friction models for liquid lubricants in view of the effects of particle shape, size, mobility and crystallographic characteristics of the particles. The main purpose of solid lubricants is to build up a continuous adherent soft or hard film in the rubbing surfaces. These films can be applied by mechanical, (electro)chemical or physical processes [7]. Due to their laminar structure, traditional solid lubricant like graphite and molybdenum have advantageous lubricating properties. However, many applications of solid lubricant are used in powder forms which reduce their tribological capacities. To maximize the tribological capabilities, the solid lubricant must be bonded to the surface of which it is lubricating [2].

Certain pure metals (e.g., In, Sn, Pb, Ag, Au, Pt, Sn, etc.) can provide low friction on sliding surfaces, because of their low shear strengths and rapid recovery as well as recrystallization [7]. They are used chiefly as solid lubricants because the attractive properties they combine are unavailable in other solid lubricants. Soft metals are generally produced as thin films on surfaces to be lubricated. Simple electroplating and vacuum evaporation can be used to deposit most of these metals as self-lubricating films, but dense and highly adherent films are produced by ion plating, sputtering, or ion-beam-assisted deposition techniques. Film-to-substrate adhesion is extremely critical for achieving long wear life or durability, especially on the surfaces of ceramic tribomaterials [7].

Over the last decade, a new class of material known as MAX phases have emerged which have shown excellent tribological behavior at high temperatures. Recent studies found that by adding MAX phases particles to metal matrix helped improved the mechanical and tribological properties of the metal matrix [8-11].

1.2 MAX Phases

The $M_{n+1}AX_n$, or MAX phases are layered, hexagonal, early transition-metal carbides and nitrides, where n = 1, 2, 3, "M" is an early transition metal, "A" is an A-group element, and "X" is C and/or N (Fig. 1.1) [12-16]. In a significant breakthrough by Barsoum and El-Raghy [20] relatively phase-pure and dense samples of Ti_3SiC_2 were synthesized. This pioneering study also revealed a material with a unique combination of metallic and ceramic properties [14].
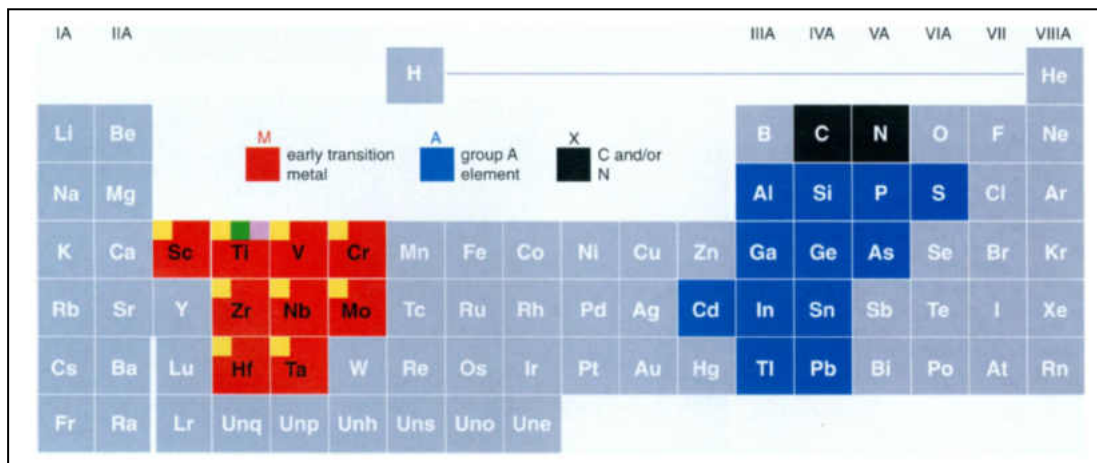
Figure 1.1: MAX phases elements on periodic table that react to form them [12].

Figure 1.2 illustrates the fundamental lattice structures of MAX phases where $M_{n+1}X_n$ layers are interleaved with pure A-group element layers. These phases are relatively soft (2-8 GPa), readily machinable, excellent thermal and electrical conductors, and damage tolerant. These solids behave like nonlinear elastic solids where during compressive cycling loading of up to 1 GPa, they can dissipate 25% of the mechanical energy at room temperature. Interestingly, at

higher temperature, they also undergo a brittle-to-plastic transition (BPT), and their mechanical behavior is dependent on deformation rate [16].
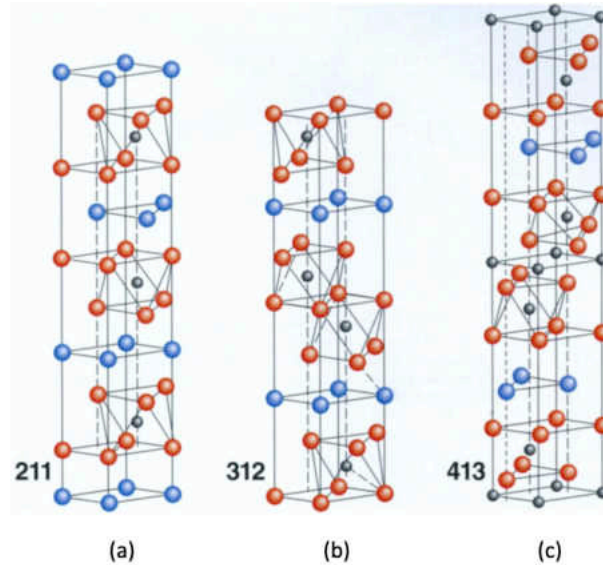
Figure 1.2: Atomic structures of (a) 211, (b) 312, and (c) 413 phases [12]

1.3 MAX Reinforced Metals (MRMs)

Metal matrix composites (MMCs) usually consist of a metal, such as aluminum or magnesium, reinforced with particulate or fibers of a ceramic material, such as silicon carbide or graphite. Compared with unreinforced metals, MMCs offer higher specific strength and stiffness, higher operating temperature, and greater wear resistance, as well as the opportunity to tailor these properties for a particular application [17]. In efforts to improving MMCs, numerous studies have incorporated MAX phases particulates in the metal matrix can be used as solid lubricant at high temperature. These composites are called Max Reinforced Metals (MRMs)

Gupta et al. [8-11, 18-19] had shown that MRMs showed promising mechanical and tribological performance as compared to pure metal matrix. This MRMs can be good candidate for applications which required high mechanical and tribological performance composite.

4

Figures 1.3-1.4 show the beneficial impacts of adding Ti_3SiC_2 to various metal matrices. MAX phases can be also used to design MAX Reinforced Polymers (MRPs) where MAX phases are incorporated into polymer matrix [22-24].

In this thesis, Ti_3SiC_2 is used as the particulate additive for manufacturing layered composites by using Ni and AlSi alloys as base metals. Ti_3SiC_2 has exceptional mechanical properties, oxidation resistance, thermal shock resistance, excellent thermal and electrical conductivity, high machinability, and low friction coefficient [16, 20].
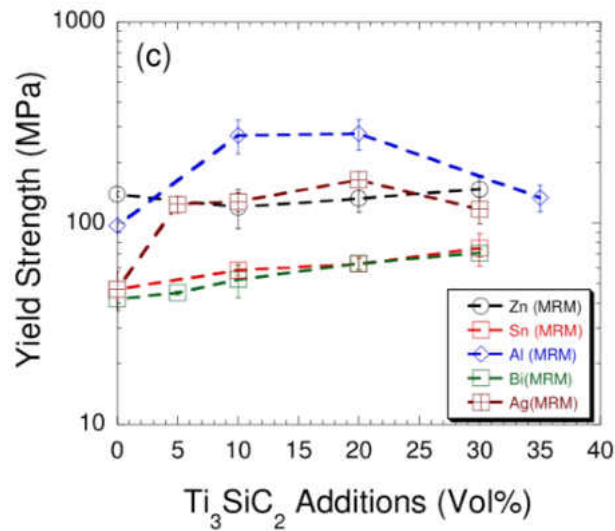
Figure 1.3: Yield Strength of various MRMs with Ti_3SiC_2 addition [11].
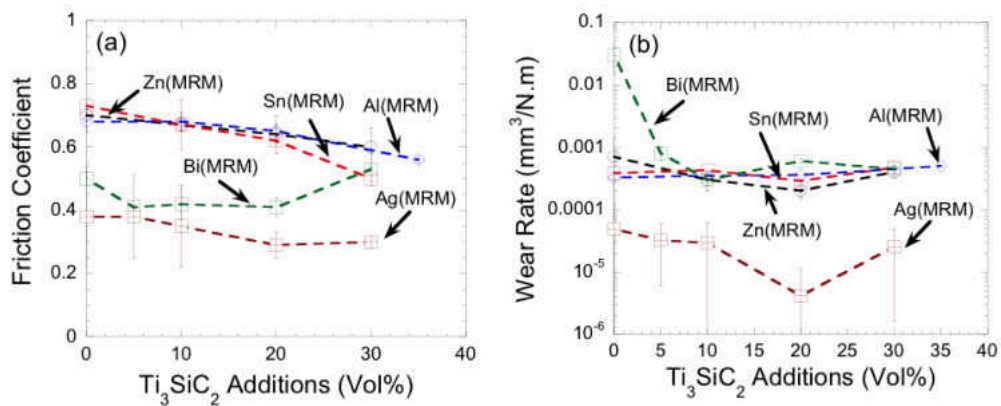
Figure 1.4 Plot of various MRMs (a) μ_m (b) WR as function of Ti_3SiC_2 additions [11].

1.4 Multilayered MAX Phases

Since the discovery of MAX Phases, there are numerous researchers who are investigating this topic, but there are no studies on MAX Phase-metal multilayered composites although there are a few studies on multilayered composites of MAX phases [25-28]. Murugaiah et al. [27] was the first team to have successfully created oriented Ti_3SiC_2 matrix by using tape casting method. However, the study reported that it was difficult to obtain a homogeneous microstructure by tape casting [27]. The authors also noticed there are significant grain growth at the surface and cracks developed in the sintered solid during grain growth [27]. Hu et al. [28] fabricated a textured Nb_4AlC_3 ceramic by slip casting in a strong magnetic field, and they sintered the cast solid by spark plasma sintering. Their research showed that the grains are uniform, and they are oriented parallel to the direction of magnetic field. In this research study, we will fabricate Metal Reinforced MAX (MRMs) multilayered composites by using the tape casting methods. The focus of this study is also to examine the properties and tribological behavior of MRMs in multilayers.

CHAPTER II
SYNTHESIS AND TRIBOLOGICAL BEHAVIOR OF NOVEL Ni-Ti$_3$SiC$_2$
MULTILAYERS COMPOSITES

2.1 Introduction to Tape Casting

Tape Casting was first introduced in the 1940s during the Second World War when there was a serious lack of quartermaster materials to produce mica capacitors. In tape casting, sometimes referred to as the doctor-blade process, the slurry is spread over a surface using a carefully controlled blade referred to as a doctor blade. As a result, films of up to hundreds of meters in length and as thin as 1 μm can be obtained, and they can be as thick as 3000 μm [1]. In tape casting, binders are often added to ceramic to create the slurry. In this study, Poly(vinyl alcohol)(PVA) is used as the binder agent since it is commonly used in dry press ceramic [2]

2.2 Experimental Details

2.2.1 Laminate Design

In this chapter, two different types of laminates were explored, namely, (a) Type I composites where composites of Ni and Ti$_3$SiC$_2$ (Ni-Ti$_3$SiC$_2$) layers were interleaved with Ni, and (b) Type II composites where Ni-Ti$_3$SiC$_2$ layers were interleaved with Al, and Ni. (Figure 2.1).
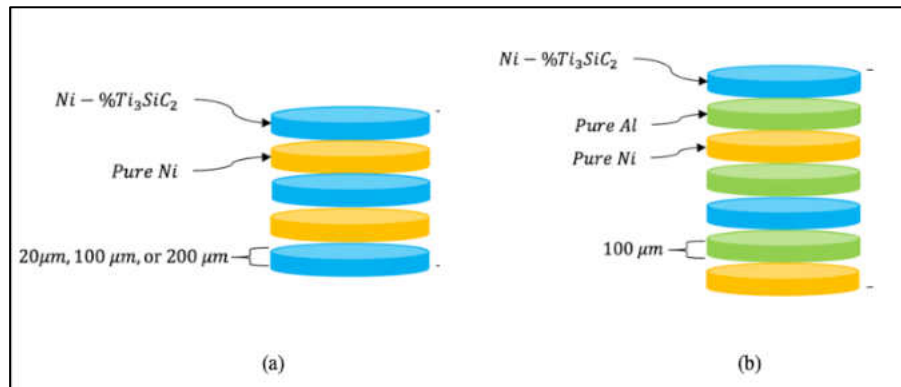
Figure 2.1 Schematics of, (a) Ni-Ti$_3$SiC$_2$/Ni, and (b) Ni-Ti$_3$SiC$_2$/Al/Ni multilayered composites.

From manufacturing perspective, each layer was cut into a circular disk to fit a 25.4 mm die (details of the manufacturing process will be described in the next section), and for experimental purpose, the sample thickness was fixed at ~4 mm. In addition, the thickness of each layer was predetermined to have a thickness of 20 μm, or 100μm, or 200 μm, respectively. Table 2.1 shown the number of layers that required to produce one ~4mm sample based on their layer thickness. Please note that in all compositions, Ni-%Ti_3SiC_2 present at the top and bottom portion of the compacts.

Table 2.1: Number of layers required to produce a compact with a thickness of ~4 mm

Thickness	Type I MMRMs		Type II MMRMs		
	Ni-%Ti_3SiC_2	Pure Metal	Ni-%Ti_3SiC_2	Pure Ni	Pure Al
20 μm	101	100	101	100	200
100 μm	21	20	11	10	20
200 μm	11	10	X		

During Type I composites, individual layer thickness was varied between 20 μm, or 100 μm, or 200 μm, and Ti_3SiC_2 concentration in the Ni-Ti_3SiC_2 was varied by 10 vol%, or 20 vol%, or 40 vol% (Tables 2.2). In the rest of this Chapter, samples will be referred by the following shorthand nomenclature; Ni-vol%Ti_3SiC_2/Ni (individual layer thickness) or Ni-vol%Ti_3SiC_2/Al/Ni (individual layer thickness), for example, Ni-20%Ti_3SiC_2/Ni (100 μm) refers to Composition B (Table 2.2).

Table 2.2: Design matrix of Ni-Ti₃SiC₂ compositions

Ni-Ti$_3$SiC$_2$ Multilayers Composition Matrix		Ni-%Ti$_3$SiC$_2$ Composition		
		10 vol% Ti$_3$SiC$_2$	20 vol% Ti$_3$SiC$_2$	40 vol% Ti$_3$SiC$_2$
LAYERS THICKNESS	20 μm	x	D	x
	100 μm	A	B	C
	200 μm	x	E	x

In type II composites, thin Aluminum layers are inserted between the Ni-Ti$_3$SiC$_2$ and Ni layers (Figure 2.1). In these composites, the concentration of Ti$_3$SiC$_2$ was kept constant at ~20 vol% in Ni-Ti$_3$SiC$_2$ layer, and the thicknesses of the laminate layers were varied between 20 μm (composition F) and 100 μm (composition G), respectively.

2.2.2 Calculation of Ti$_3$SiC$_2$ Concentration in Composite

The concentration of Ti$_3$SiC$_2$ are fixed at 10%, 20%, and 40% in each layer of Ni-Ti$_3$SiC$_2$ in the matrix. It is important to note that these concentrations are based on the vol (%) content of Ti$_3$SiC$_2$ in the Ni-Ti$_3$SiC$_2$ individual layers but not of the vol% of the entire monolithic composites. In other words, the overall volume content of Ti$_3$SiC$_2$ in multilayered composites will be different from the isotropic composites with similar chemistry of the individual layers. For example, an isotropic Ni-10%Ti$_3$SiC$_2$ with 4 mm thickness will have 10 vol% Ti$_3$SiC$_2$ dispersed throughout the ~4 mm composite (Fig. 2.2a), however in multilayered composites, 10% Ti$_3$SiC$_2$ is referred to the concentration of each Ni- Ti$_3$SiC$_2$ layers (Fig. 2.2b)
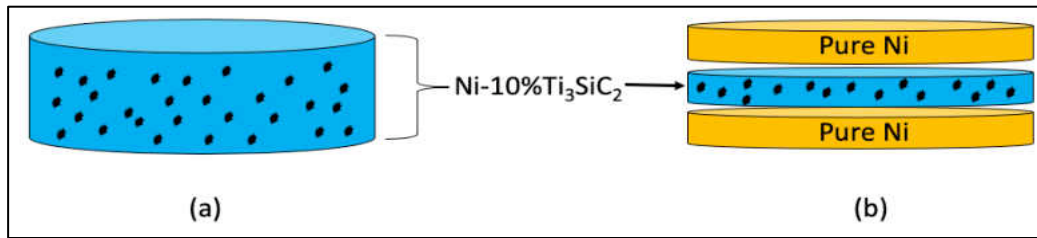
Figure 2.2: Concentration of Ti_3SiC_2 in: (a) Isotropic $Ni-Ti_3SiC_2$ composites, (b) multilayered $Ni-Ti_3SiC_2$ composites

Therefore, multilayered composites will contain approximately half the volume of MAX phases as compared to the isotropic composites. Table 2.3 shows the theoretical calculation of Ti_3SiC_2 in the multilayered $Ni-Ti_3SiC_2$ composites. The Ti_3SiC_2 concentration mention in this thesis will be 10%, 20%, 40% in the individual layers, not volume of the composites.

Table 2.3: Concentration of $Ni-Ti_3SiC_2$ in multilayered $Ni-Ti_3SiC_2$ composites

COMPOSITION	THICKNESS	Ti_3SiC_2 CONCENTRATION (%)	
		Isotropic $Ni-Ti_3SiC_2$	Multilayered $Ni-Ti_3SiC_2$
$Ni-10\%Ti_3SiC_2$ / Ni		10%	5.01%
$Ni-20\%Ti_3SiC_2$ / Ni	100 μm	20%	10.24%
$Ni-40\%Ti_3SiC_2$ / Ni		40%	20.50%
$Ni-20\%Ti_3SiC_2$ / Ni	20 μm	20%	10.05%
$Ni-20\%Ti_3SiC_2$ / Ni	200 μm	20%	10.47%
$Ni-20\%Ti_3SiC_2$ / Al / Ni	20 μm	20%	5.36%
$Ni-20\%Ti_3SiC_2$ / Al / Ni	100 μm	20%	5.07%

2.2.3 Manufacturing Process

Initially, binder solution was mixed by dissolving ~20g Poly Vinyl Alcohol (PVA)(98-99% hydrolyzed, Aldrich Chemistry, St. Louis, MO) in ~80 g Distilled (DI) Water. Thereafter, Ti_3SiC_2 powder (-325 mesh, Kanthal, Halllstanhammar, Sweden) was mixed with Ni powder (-325 mesh, Alfa Aesar, Haverhill, MA) by ball milling (8000 M mixer Mill, SPEX SamplePrep, Metuchen, NJ) for 5 minutes. Table 2.4 shows the calculation used for fabricating each composite design.

Table 2.4: Weight fraction of Ti$_3$SiC$_2$ and Ni used for designing composites

Component	Vol %	Density (g/cm3)	Component Density (g/cm3)	Components Vol (cm3)	Components Weight (g)
Ni	0.9	8.908	8.469	1.824	16.246
Ti$_3$SiC$_2$	0.1	4.52		0.203	0.916
Ni	0.8	8.908	8.030	1.621	14.441
Ti$_3$SiC$_2$	0.2	4.52		0.405	1.832
Ni	0.6	8.908	7.157	1.216	10.831
Ti$_3$SiC$_2$	0.4	4.53		0.811	3.672

The slurry used for tape casting was designed by mixing Ni powder and the PVA solution in 60:40 weight ratio by ball milling for ~5 min. The slurry was then the poured into the tape casting machine (MSK-AFA-111-110, Automatic Thick Film Coater, MTI Corp, Richmond, CA) with a speed set at 20 cm/min, and the doctor blade was set to the desired gap thickness (Fig. 2.2c). Similarly, Ni- Ti$_3$SiC$_2$ and Al layers were also cast by using the above-mentioned process.

Figure 2.2c: Tape casting set up for casting individual layers

Initially, the tape cast film was allowed to dry at room temperature for ~12 h until the material can be handled. However, it was observed that the dried sample has a tendency to warp which makes the lamination process cumbersome and difficult (Figure 2.3a). In order to combat

the problem of warping, clean pieces of wood were placed on top of the film after 2.5-3 h drying

in ambient air (Fig. 2.3b). Figure 2.3c illustrates a uniform tape cast film after drying.
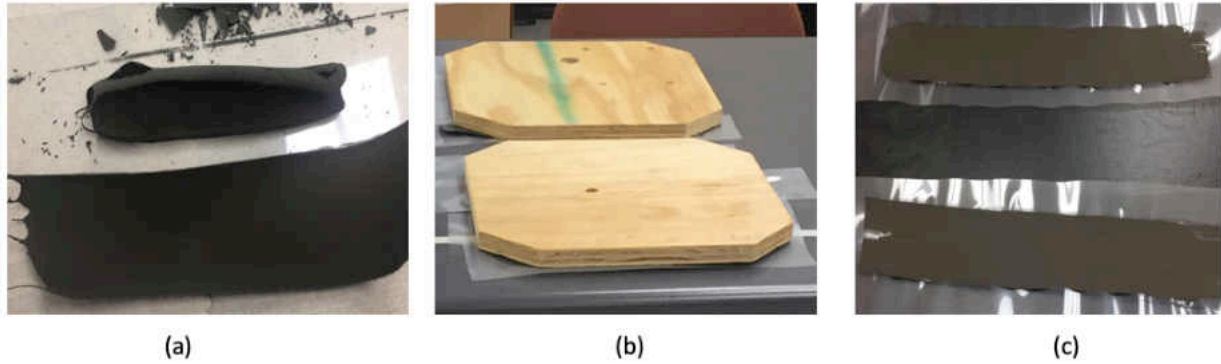
Figure 2.3: (a) Warping during drying process, (b) wood block used for restraining sample, and (c) the flat tape cast film after drying.

A simple 1" (25.4 mm) diameter punch from a local hobby store was used to cut the

cured thin film according to the diameter of the die . (Figure 2.4). The samples were then loaded

into a 25.4 mm diameter dry pressing die (1701064, MTI Corp, Richmond, CA) according to the

laminate design (Table 2.1).

Figure 2.4: (a) Punch die used for fabricating 1" samples, and (b) examples of laminates after

The layers were stacked into the die, and the die was then preloaded in a hot press (TF

1200X, MTI Corp, Richmond CA) (Figure 2.5a) at ~1.49 MPa, thereafter the die was heated at

the rate of 10 $^\circ$C/min to 150 $^\circ$C, the die was then held for 5 min, and the die was then laminated

by hot pressing at 150 °C for ~5 min by using a uniaxial pressure of ~119.6 MPa. The die was cooled to the room temperature, thereafter the die was heated to 650 °C at 10 °C/min under a constant pressure of 1.49 MPa. The die was allowed to stabilize at temperature 650 °C for 5 min, thereafter the die was hot pressed at ~142 MPa for ~5 min. The die was then cooled to RT, and the sample was removed from the die (Figure 2.5b).
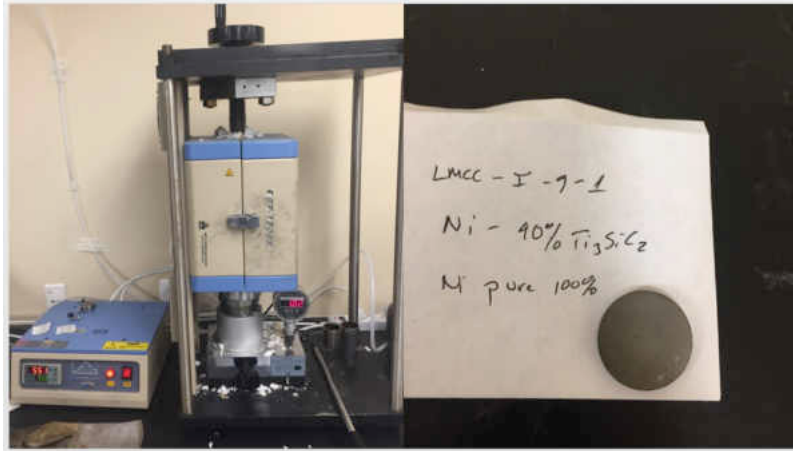
Figure 2.5: (a) Hot press used for the manufacturing process, and (b) an example of a hot-pressed sample.

2.3 Post Processing and Testing

The density of the sintered samples was measured on polished samples. All the samples were machined into 3 mm x 3 mm x 3mm or 4 mm x 4 mm x 4mm cubes by using a low speed saw (ISOMET low speed saw, Buehler, Lake Bluff, IL) with diamond coated blade (IsoCut Wafering Blades, Buehler, Lake Bluff, IL). The samples were then carefully examined to ensure that the orientation of the samples were correct. Figure 2.6 shows the orientation of the composite samples at which they were tested, for example, if the layers are aligned parallel or perpendicular to the surface then it will be referred to parallel or perpendicular orientation, respectively (this notation will be used in rest of the thesis).
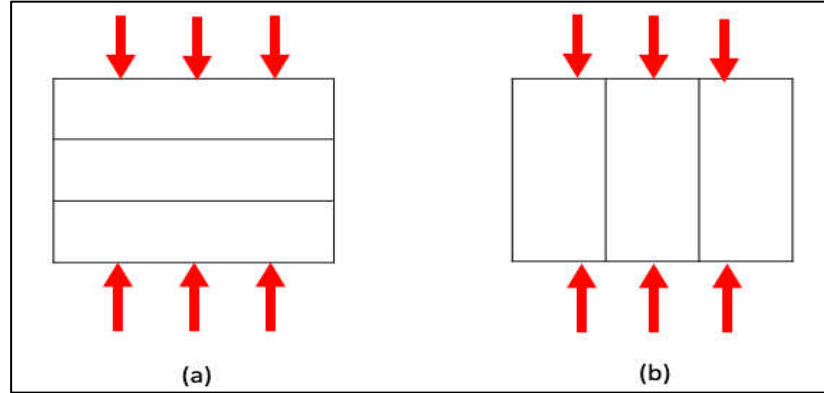
Figure 2.6: Orientation of the composite (a) parallel and (b) perpendicular layers.

Theoretical (true) density of Ti_3SiC_2, Ni, and/or Al were used to calculate the theoretical density (ρ_T) of the individual layers. The theoretical density of all the composite samples (ρ_{cT}) was then determined by using the rule of mixture calculations which was based on the nominal composition of each composite system. The experimental density (ρ_E) of the composites was calculated from the mass and dimensions of each sample after hot pressing. Thereafter, the porosity (P) of the sample was determined by the Eq, 1.

$$P = \left(1 - \frac{\rho_E}{\rho_{cT}}\right) \text{ x } 100 \text{ ---(I)}$$

For each composition, a set of 3 samples were then tested in compression in parallel and perpendicular orientation by using a mechanical testing unit (Shimadzu AD-IS UTM, Shimadzu Scientific Instruments Inc., Columbia, MD) at a deflection rate of 1 mm/min on cube samples (~3 mm x ~3 mm x ~3 mm). The maximum compressive stress at which a sample fractures is referred to as Ultimate Compressive Strength (UCS) in the text.

Due to experimental limitations, stress versus displacement plots are reported as the actual strain during mechanical testing could not be determined. In the paper, the yield strength is defined when stress versus displacement plot transitions from the linear to non-linear regime. The linear

region of the composites had a regression fitting of $R^2 > 0.95$. For each composite, an average of 3 yield strength measurements is reported in the text [3-7].

The tribological behavior of the samples were investigated by using a block-on-disc tribometer (CSM Instruments SA, Peseux, Switzerland) against alumina disks. The experiment conditions used during these studies were 5 N, ~50 cm/s linear speed, ~10 mm track radius, and a sliding distance of 1000 m, respectively. All the Ni-Ti$_3$SiC$_2$ blocks were also polished to a ~1 µm finishing which were confirmed by using a surface profilometer (Surfcom 480A, Tokyo Seimitsu Co. Ltd., Japan). After performing the tribological testing for each composition, the μ_{mean} was then calculated by averaging the mean results obtained from the three data sets of similar Ni-Ti$_3$SiC$_2$ compositions. The mass of the samples and substrates were measured before and after the testing by using a weighing scale (Model XA82/220/2X, Radwag Balances and Scales, Poland). The specific wear rate (WR) was calculated from:

$$WR = (m_i - m_f)/(\rho.N.d) \text{ --------------------------(II)}$$

where, m_i is the initial mass, m_f is the final mass, ρ is density of the composite, N is the applied load, and d is the total distance traversed by the sample during the tribology testing [3-7]. The total WR from both the counterparts is reported in the text.

After tribological testing, alumina balls were coated with Au/Pd by using a Balzers SCD 030 sputter coater (BAL-TEC RMC, Tucson AZ USA), and then mounted on aluminum mounts for microscopy investigations. For all the samples, Secondary electron (SE) and Backscattered Electrons (BSE) images were obtained by using a JEOL JSM-6490LV Scanning Electron Microscope (JEOL USA, Inc., Peabody, MA) and X-ray information was also determined by using a Thermo Nanotrace Energy Dispersive X-ray detector with a NSS-300e acquisition engine. During BSE and X-ray analysis of a region, if that region was determined to be chemically uniform

at the micron level then it was identified with two asterisks as *microconstituent* to emphasize that region is not necessarily single phase. In addition, the accuracy of measuring C is quite low during chemistry analysis by X-ray detector in SEM, thus the presence of C in microconstituents will be designated as $\{C_x\}$ [3-7].

2.4 Result and Discussion

2.4.1 Microstructure Analysis

Figures 2.7-2.8 show the SEM micrographs of Ni-Ti$_3$SiC$_2$/Ni multilayered composites. By analyzing the micrographs, it can be summarized that, (a) all the layers are uniform and, (b) Ti$_3$SiC$_2$ particles are homogenously distributed in the microstructure with minimal reaction. However, the introduction of Al as an interleaving layer between Ni-Ti$_3$SiC$_2$ and Ni in the composite matrix caused interfacial reaction at the interfacial boundary between Ni and Al (Figure 2.9). Like Ni-Ti$_3$SiC$_2$/Ni multilayered composites, all the layers were observed to be uniform, and Ti$_3$SiC$_2$ particulates were uniformly dispersed in the Ni-matrix.
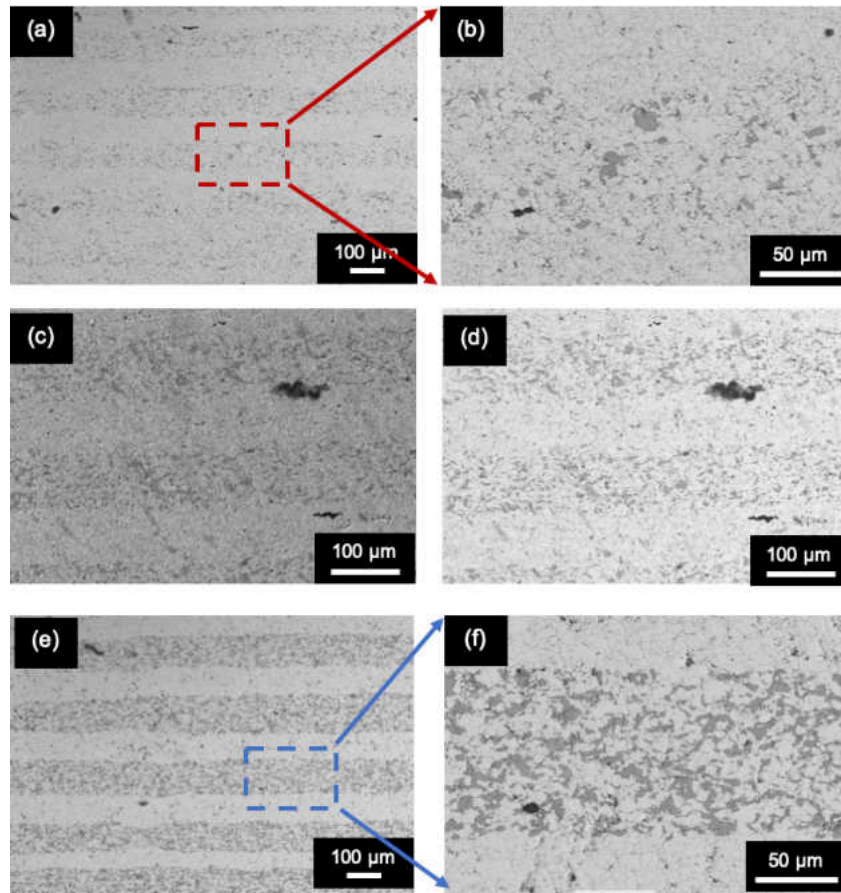
Figure 2.7: SEM microstructure of, (a) Ni-10%Ti$_3$SiC$_2$/Ni (100 μm) in BSE, (b) BSE image at higher magnifications, (c) Ni-20%Ti$_3$SiC$_2$/Ni (100 μm) in SE, (d) BSE of the same region, (e) Ni-20%Ti$_3$SiC$_2$/Ni (100 μm) in BSE, and (f) Ni-20%Ti$_3$SiC$_2$/Ni (100 μm) in BSE at higher magnifications.
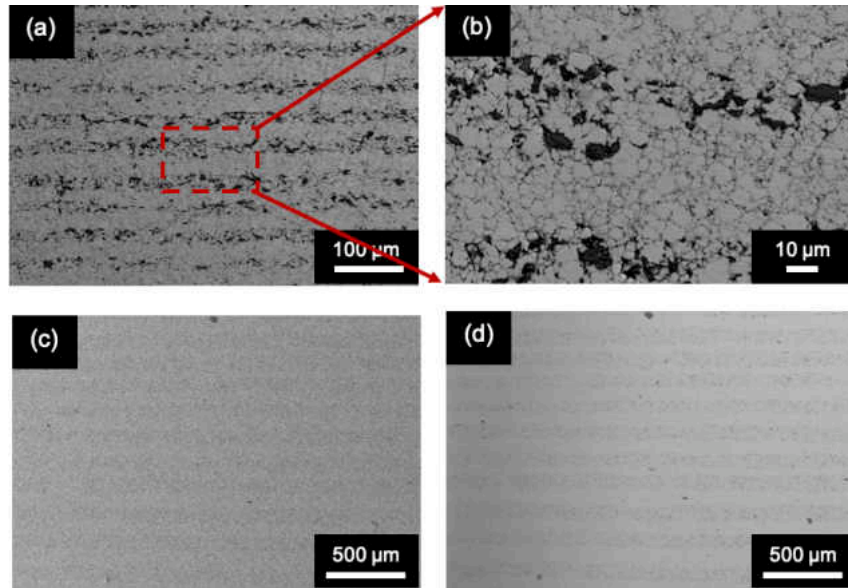
Figure 2.8: SEM microstructures of, (a) Ni-20%Ti$_3$SiC$_2$/Ni (20 µm) in BSE, (b) Ni-20%Ti$_3$SiC$_2$/Ni (20 µm) in BSE at higher magnifications, (c) Ni-20%Ti$_3$SiC$_2$/Ni (200 µm) in SE, and (d) BSE of the same region.
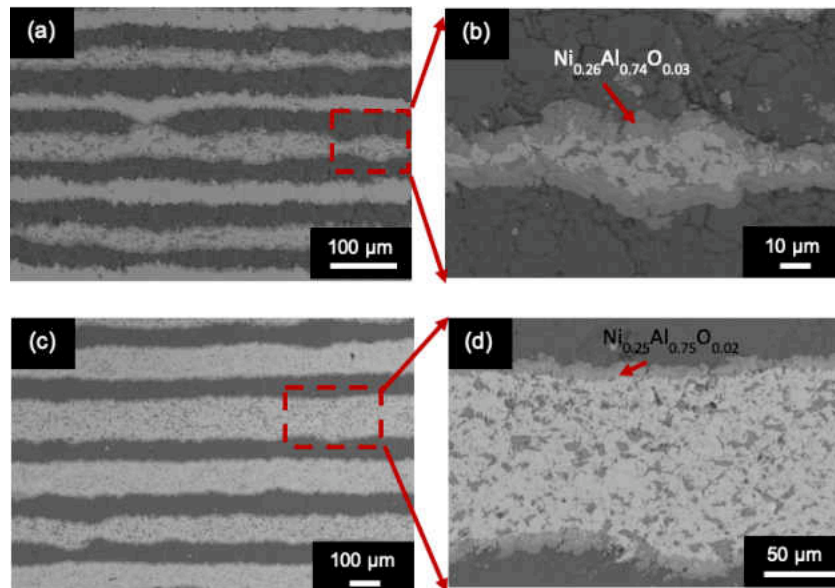
Figure 2.9: SEM microstructure of, (a) Ni-20%Ti$_3$SiC$_2$/Al/Ni (20 µm) in BSE, (b) higher magnification in BSE, (c) Ni-20%Ti$_3$SiC$_2$/Al/Ni (100 µm) in BSE, and (d) higher magnification in BSE.

2.4.2 Mechanical Analysis

Figure 2.10 shows the stress versus displacement plots for all composites. The Ni-Ti$_3$SiC$_2$ composites showed, in both directions, ductile and gradual failure with signs of damage recovery. In all plots, the failure in both direction happened in similar manner. In the type II composites, the addition of Al into the composite matrix caused the composites to become ductile and the failure was gradual in both orientations. Figure 2.11 shows the Ultimate Compressive Strength (UCS) of all the tested composites. In Type I composites, the UCS marginally increased in Ni-20%Ti$_3$SiC$_2$/Ni (100 µm) in parallel direction, thereafter the UCS decreased, whereas in the perpendicular orientation the UCS decreased gradually. Interestingly, when the composition was fixed at 20 vol% in the Ni-Ti$_3$SiC$_2$ layer, and layer thickness was varied in Ni-Ti$_3$SiC$_2$/Ni composites, the UCS increased in the parallel direction whereas in the perpendicular direction there was no significant change. In Type II composites (Figure 2.11c), where the concentration of Ti$_3$SiC$_2$ was fixed at 20 vol%, the UCS increased in both orientation as the layer thickness increased. This study shows that Al layers are good adhesive to increase the UCS of these materials.
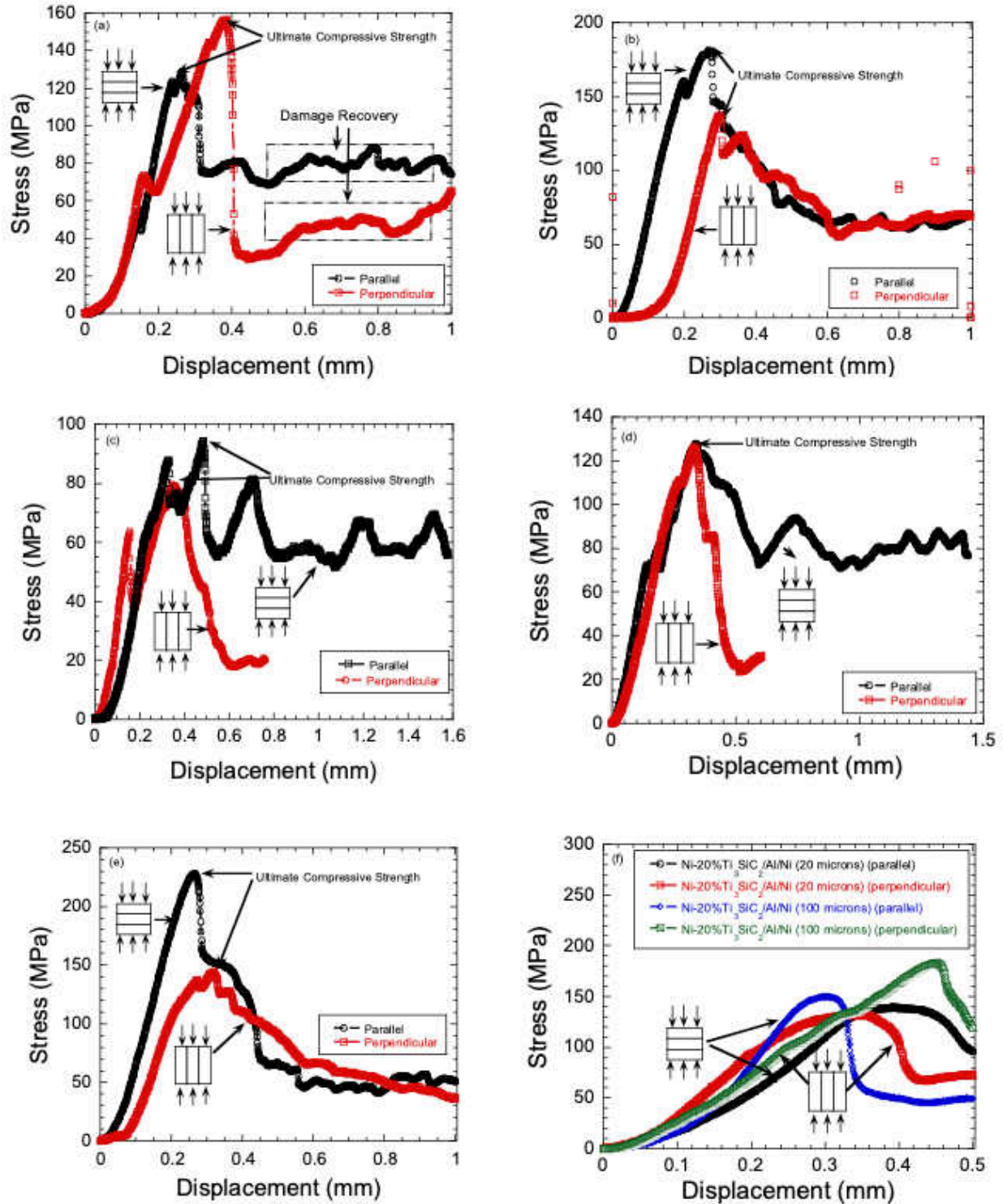
Figure 2.10: Plot of compressive stress versus displacement of, (a) Ni-10%Ti₃SiC₂/Ni (thickness of laminate is 100 μm), (b) Ni-20%Ti₃SiC₂/Ni (thickness of laminate is 100 μm), (c) Ni-40%Ti₃SiC₂/Ni (thickness of laminate is 100 μm), (d) Ni-20%Ti₃SiC₂/Ni (thickness of laminate is 20 μm), (e) Ni-20%Ti₃SiC₂/Ni ((thickness of laminate is 200 μm), and (f) Ni-10%Ti₃SiC₂/Al/Ni composites with different thicknesses.
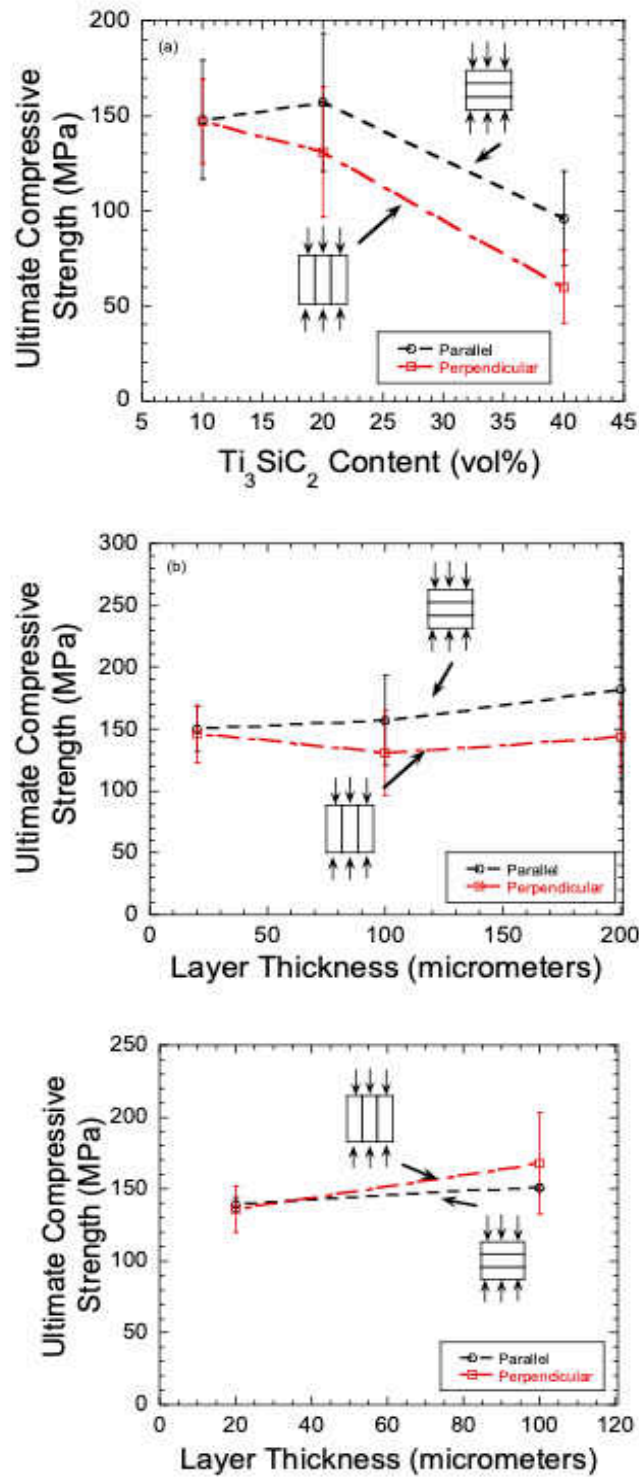
Figure 2.11: Plot of Ultimate Compressive Strength (UCS) versus Ti_3SiC_2 content in, (a) Ni-Ti_3SiC_2 (100 μm), (b) Ni-20%Ti_3SiC_2/Ni, and (c) Ni-Ti_3SiC_2/Al/Ni multilayered composites.

2.4.3 Tribological Behavior of Ni-Ti$_3$SiC$_2$ Composites

Figure 2.12 shows the plot of μ and WR in Ni-20%Ti$_3$SiC$_2$/Ni (Type I) composites. As the thickness was increased, the μ slightly increased in the parallel direction from ~0.43 in 20 μm to ~0.46 in 100 μm, thereafter it decreased to ~0.43 when the layer thickness was increased to 200 μm . However, in perpendicular direction the same composites showed a steady decline in μ from ~0.46 to ~0.39 when the layer thickness was varied from ~20 μm to ~200 μm, respectively. The WR also showed interesting behavior, for example in Ni-20%Ti$_3$SiC$_2$/Ni (20 μm) samples there were no significant difference between the WR in parallel and perpendicular orientation. However, in the perpendicular orientation, the WR decreased from 2 x 10^{-3} mm^3/Nm in Ni-20%Ti$_3$SiC$_2$/Ni (20 μm) to 4 x 10^{-4} mm^3/Nm Ni-20%Ti$_3$SiC$_2$/Ni (100 μm) and 3 x 10^{-4} mm^3/Nm at Ni-20%Ti$_3$SiC$_2$/Ni (200 μm), respectively. However, in the parallel direction, the WR decreased from 2 x 10^{-4} mm^3/Nm in Ni-20%Ti$_3$SiC$_2$/Ni (20 μm) to 5 x 10^{-4} mm^3/Nm in Ni-20%Ti$_3$SiC$_2$/Ni (100 μm), but then sharply increased to 2 x 10^{-3} mm^3/Nm in Ni-20%Ti$_3$SiC$_2$/Ni (200 μm). This behavior can be explained by the following hypothesis: (1) in the parallel direction, the Ti$_3$SiC$_2$ containing Ni-Ti$_3$SiC$_2$ layer is interleaved with Ni layers thus by increasing the layer thickness, it may take longer for the MAX phases to create a lubricious tribofilm, and (2) in the perpendicular direction, the MAX phases are always present in the contact area thus they are effectively able to lubricate the dry contacts as compared to the former case. More studies are needed to validate this hypothesis.
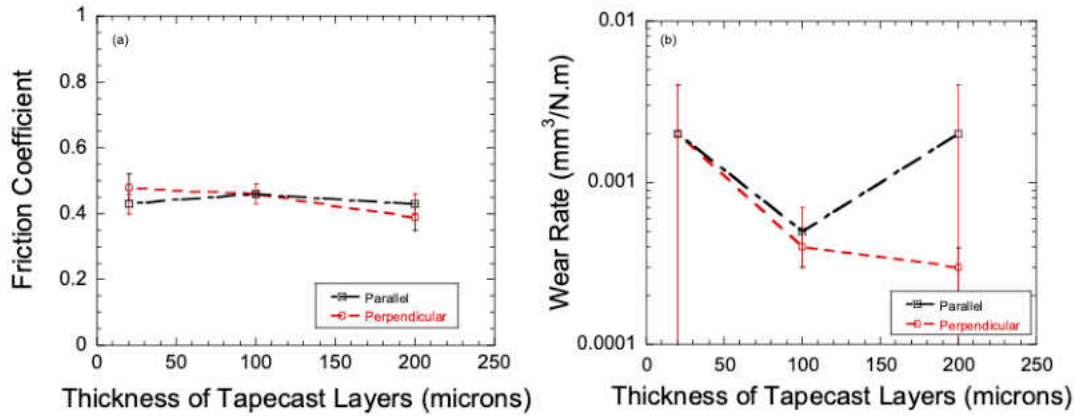
Figure 2.12: Plot of, (a) friction coefficient, and (b) WR of Ni-20%Ti$_3$SiC$_2$/Ni multilayered composites with laminate of different thicknesses.

Figure 2.13 summarizes the μ and WR of Ni-Ti$_3$SiC$_2$/Ni (100 μm) composites as compared to monolithic Ni-Ti$_3$SiC$_2$, Ni-MoAlB, and Ni-20%Ti$_3$SiC$_2$ (fabricated by presureless and constrained sintering for comparison) when the concentration of Ti3SiC2 was varied from 10-40 vol% Ti$_3$SiC$_2$ in the individual layers [8, 9]. For all the vol%, both the perpendicular and parallel orientation of the composite have lower μ than the monolithic Ni-Ti$_3$SiC$_2$ and Ni-MoAlB. This study clearly shows that layering helps in reducing both the WR and μ by facilitating the shear between individual layers. More studies are needed to understand the effect of porosity on the tribological behavior of these composites.
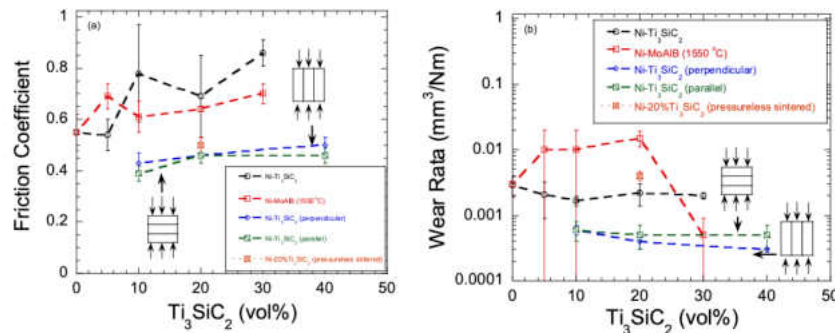
Figure 2-13: Plot of, (a) friction coefficient, and (b) wear rate as a function of Ti$_3$SiC$_2$ content in Ni- Ti$_3$SiC$_2$/Ni composites (laminate thickness in all composites was 100 μm) [8, 9].

Figure 2.14 shows the comparison of μ and WR between different compositions. The plot clearly shows that there is an increased in μ due to the addition of Al-layers in the compositions F and G. Interestingly, the WR showed an increase in perpendicular direction in compositions F and G. However, when compared to the parallel direction, the Composition G showed a decreased in WR. The possible reason is that the Al-layers are effective in shearing during parallel orientation as compared to the perpendicular orientation which can cause a lower WR.
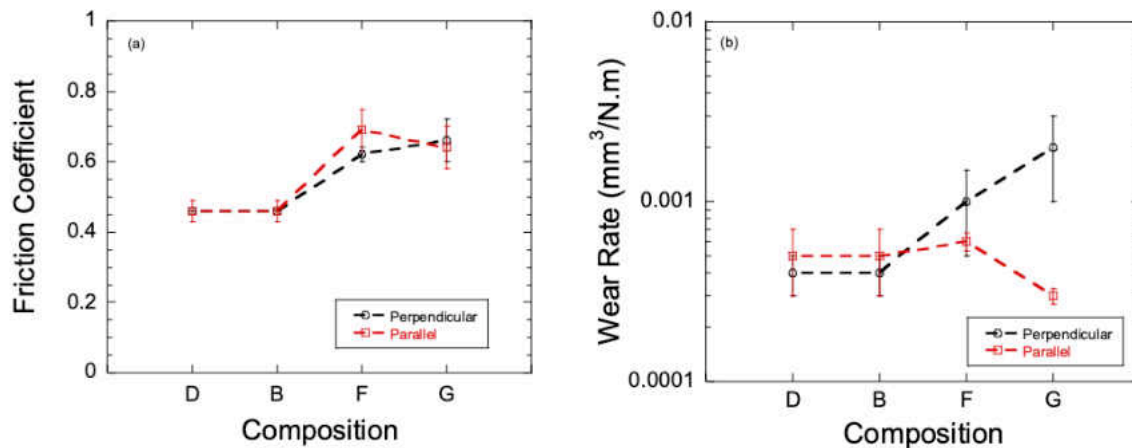
Figure 2.14: Comparative plot of, (a) friction coefficient, and (b) WR (Table 2.2).

Figures 2.15a-d show Ni-20%Ti$_3$SiC$_2$/Ni (100 μm) composite and alumina surfaces after tribological testing in the parallel orientation. On the both surfaces, there are signs of abrasive and oxidative wear present. For example, the tribo-surface of Ni-20%Ti$_3$SiC$_2$/Ni (100 μm) was partially oxidized (*NiO$_{0.003}${C$_x$}*), Figure 2.15b) and powdered wear debris (*Ni$_{0.96}$Ti$_{0.03}$Si$_{0.01}$O$_{0.027}${C$_x$}*, Fig. 2.15d) was observed on the alumina surface, respectively. Similarly, Figs. 2.16a-d show the Ni-20%Ti$_3$SiC$_2$/Ni (100 μm) composite in the perpendicular direction. Similar oxidative tribochemical reactions and powdered/smeared wear debris were observed on these surfaces too.
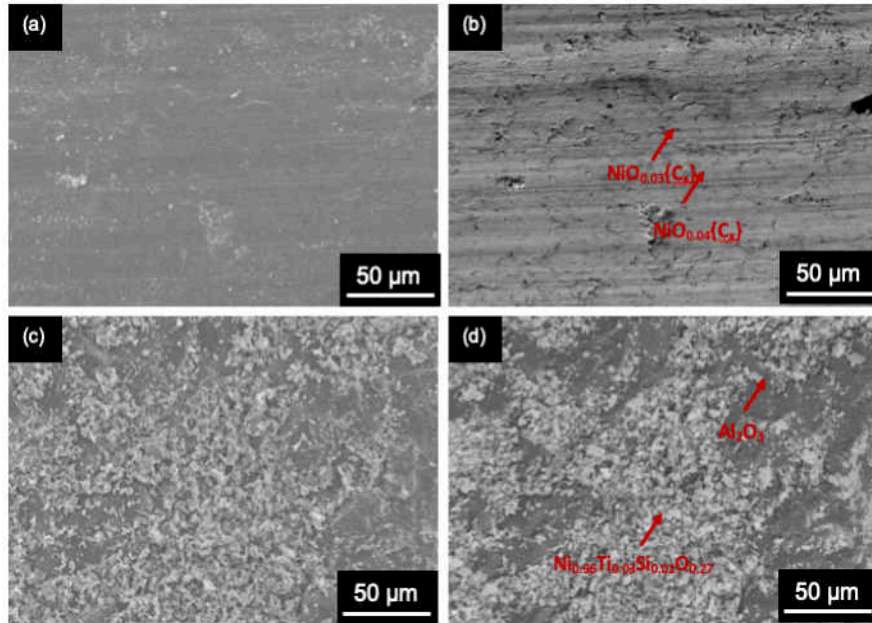
Figure 2.15: SEM micrographs of, (a) Ni-20%Ti$_3$SiC$_2$/Ni (100 µm) surface in SE, (b) BSE of the same region, (c) alumina surface in SE, and (d) BSE of the same region after tribological testing in parallel orientation.
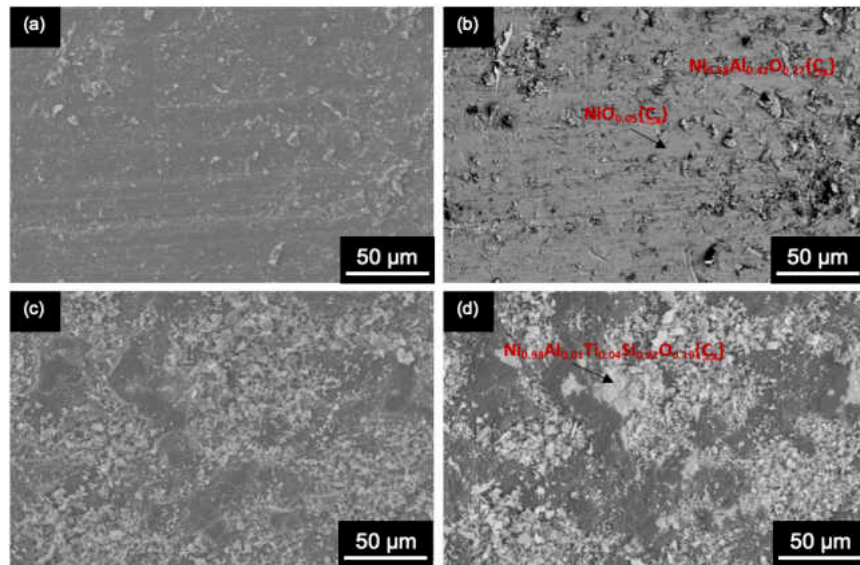
Figure 2.16: SEM micrographs of, (a) Ni-20%Ti$_3$SiC$_2$/Ni (100 µm) surface (perpendicular to the casting direction) in SE, (b) BSE of the same region, (c) alumina surface in SE, and (d) BSE of the same region after tribological testing in perpendicular orientation.

Figures 2.17-2.18 show Ni-20%Ti$_3$SiC$_2$/Al/Ni (100 μm) (Type II) composite in both parallel and perpendicular orientation after testing, respectively. All the surfaces showed signs of heavy abrasive and oxidative wear.
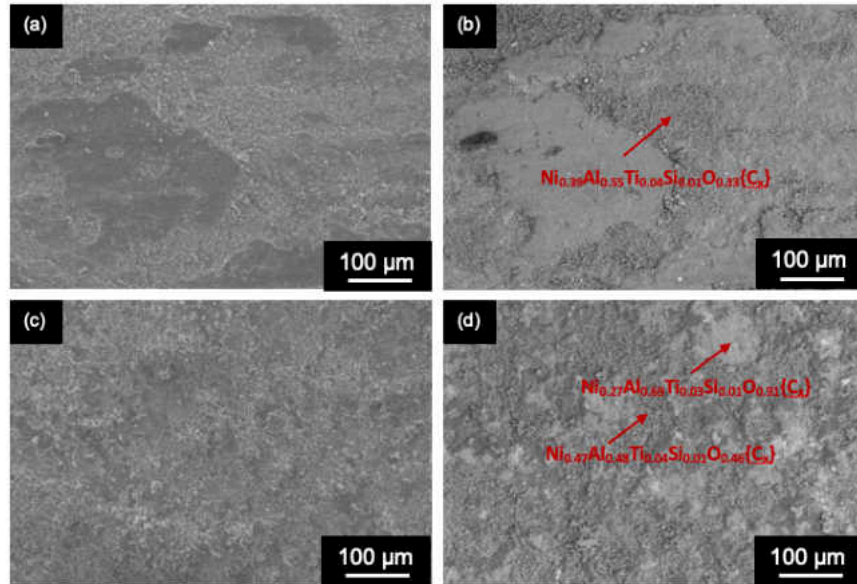
Figure 2.17: SEM micrographs of, (a) Ni-20%Ti$_3$SiC$_2$/Al/Ni (100 μm) surface (parallel orientation) in SE, (b) BSE of the same region, (c) alumina surface in SE, and (d) BSE of the same region after tribological testing
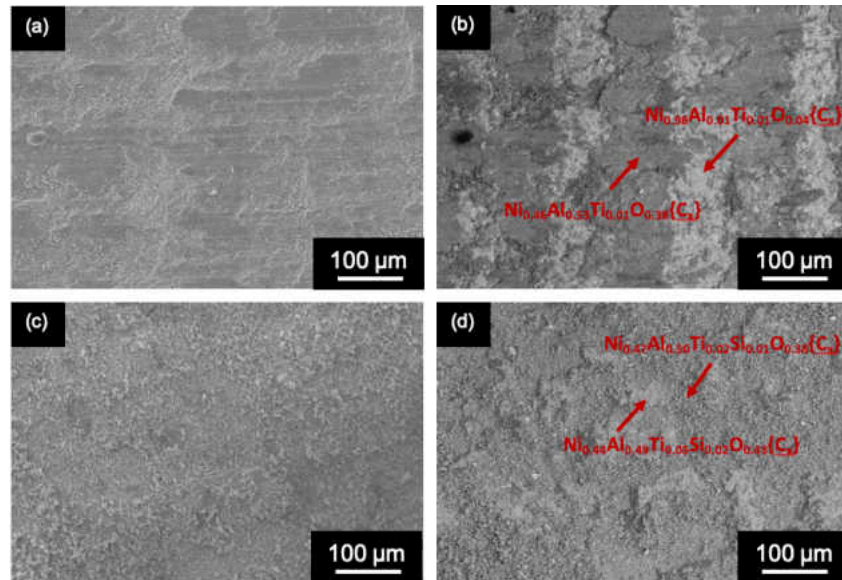
Figure 2.18: SEM micrographs of, (a) Ni-20%Ti$_3$SiC$_2$/Al/Ni (100 μm) surface (perpendicular to the casting direction) in SE, (b) BSE of the same region, (c) alumina surface in SE, and (d) BSE of the same region after tribological testing

26

2.4.4 Conclusions

Metal Reinforced MAX (MRMs) based multilayered composite was successfully fabricated for the first time. Detailed SEM studies showed that Ni-Ti$_3$SiC$_2$ particulates are well distributed in the Ni-matrix with little or no interfacial reactions. However, there were interfacial reaction to between Ni and Al in Type II composites. This study showed that the orientation of the layers affects both the mechanical and tribological performance of the composites. During tribological study, all surface showed signs of heavy abrasive and oxidative wear.

CHAPTER III
SYNTHESIS AND TRIBOLOGICAL BEHAVIOR OF NOVEL $AlSi - Ti_3SiC_2$ MULTILAYERS COMPOSITES

3.1 Introduction to Aluminum Silicon (AlSi) Alloys

Mahallawy et al. [1, 2] had reported that the combination of high purity commercial aluminum with the AlSi metal matrix composite by using the accumulative roll bonding (ARB) was effective in increasing the tensile strength and hardness. As a background, Aluminum Silicon (AlSi) alloys are widely used in automotive industries as a basic foundry alloy owing to a very attractive combination of mechanical, physical, and casting properties [3]. More particularly, this alloy is of great importance to engineering industries as it has high strength to weight ratio, high wear resistance, low density, and low coefficient of thermal expansion. Al-12%Si alloy usually exhibits low formability at ambient temperatures because of the coarse plate-like nature of the Si phase that lead to premature crack initiation and fracture in tension [2].

In this chapter, MAX phases will be introduced in the AlSi alloy matrix to enhance the alloy characteristics.

3.2 Experimental Detail

3.2.1 Sample Preparation

Sample preparation procedures are similar to section 2.3.1 in previous chapter. The component for this study are: Aluminum Silicon (Al-12%Si) (-325 mesh, Alfa Aesar, Ward Hill, MA), Ti_3SiC_2 (-325 mesh, Kanthal, Hallstahammar, Sweden) and pure Aluminum (-325 mesh, 99.5%, Alfa Aesar, Ward Hill, MA) powders. Aluminum Silicon (Al-12%Si) alloy will be referred to as AlSi in the text. Components weight are based on the percentage volume of each material. Table 3.1 shown the calculation of each composite. The 12.7 mm die were used in this study. In this study, the composites will be type I composite as shown in figure 3.1.

Table 3.1 Components weight of Ti$_3$SiC$_2$ and AlSi

Components	Components Weight used (g)	Density (g/cm^3)	Volume (cm^3)	Vol (%)	Density (g/cm^3)
Al	4.827	2.75	1.755	100	2.75
AlSi	5.364	2.7455	1.9537	100	2.745
AlSi	5.113	2.7455	1.8624	94.84	
Ti$_3$SiC$_2$	0.458	4.52	0.1013	5.16	2.837
AlSi	4.306	2.7455	1.5684	79.47	
Ti$_3$SiC$_2$	1.832	4.52	0.4053	20.53	3.110
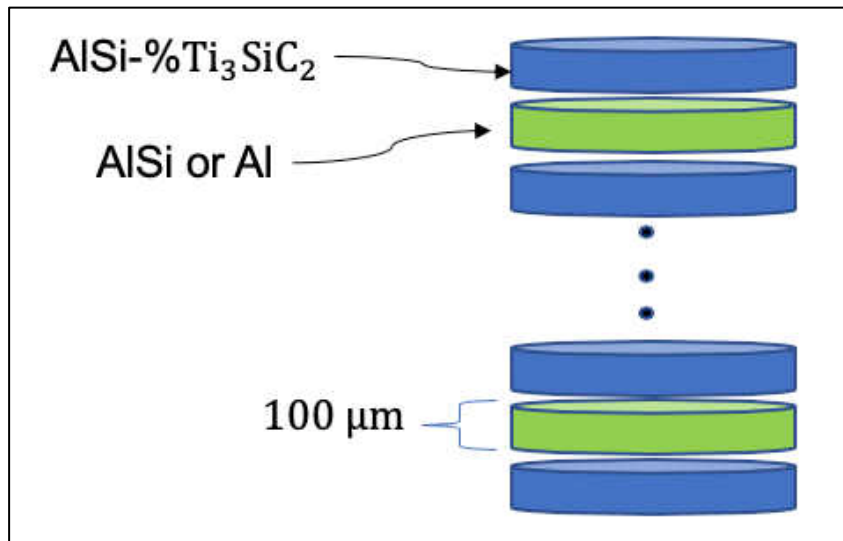
Figure 3.1 Schematic design of AlSi-%Ti₃SiC₂ / AlSi or Al Multilayered Composites

3.2.2 Sintering

The tape cast disks were inserted into a 12.7 mm die for hot pressing. The die was then loaded into a hot press (TF 1200X, MTI Corp, Richmond CA) at 29.9 MPa, and heated to 200 °C at the rate of 10 °C/min. After holding at 200 °C for 10 min, the uniaxial pressure on the dies was increased to 254.3 MPa and held for 10 min to laminate the layers. After the completion of

lamination process, the temperature was then increased from 200 °C to 550 °C by heating at rate of 10 °C /min under a constant pressure of 29.9 MPa. The die was then held at 550 °C for 5 min, thereafter the sample was hot pressed at 284.2 MPa for an additional ~10 min. Thereafter, the die was allowed to cool to room temperature and the sample was demolded from the die.

3.2.3 Post Processing and Characterization

Please refer to the section 2.3 for post-treatment and characterization methodologies. In this chapter, the tribological behavior of the samples was investigated by using a block-on-disc tribometer (CSM Instruments SA, Peseux, Switzerland) against alumina disks like it was mentioned in the last Chapter. During preliminary testing, it was observed that AlSi-Ti_3SiC_2/AlSi or AlSi-Ti_3SiC_2/Al composites were not as wear resistant as the Ni-Ti_3SiC_2 composites thus the sliding distance was changed from the previous chapter, for example in AlSi-Ti_3SiC_2/AlSi composites in parallel and perpendicular orientation, it was ~500 and ~100 m, respectively, and in AlSi-Ti_3SiC_2/Al composites in parallel and perpendicular orientation, it was at least ~100 m and ~50 m, respectively. The other experiment conditions used during these studies were 5 N, ~50 cm/s linear speed, and ~10 mm track radius. The experimental details for other studies are similar to the last Chapter.

3.3 Results and Discussion

3.3.1 Microstructure Analysis

Figures 3.2 – 3.3 summarize the SEM micrographs of AlSi-Ti_3SiC_2/AlSi and AlSi-Ti_3SiC_2/Al multilayered composites. Further analysis of the images showed that the hot-pressed layers are, (a) uniform and (b) Ti_3SiC_2 particles are homogenously distributed in the microstructure with little or no interfacial reaction.
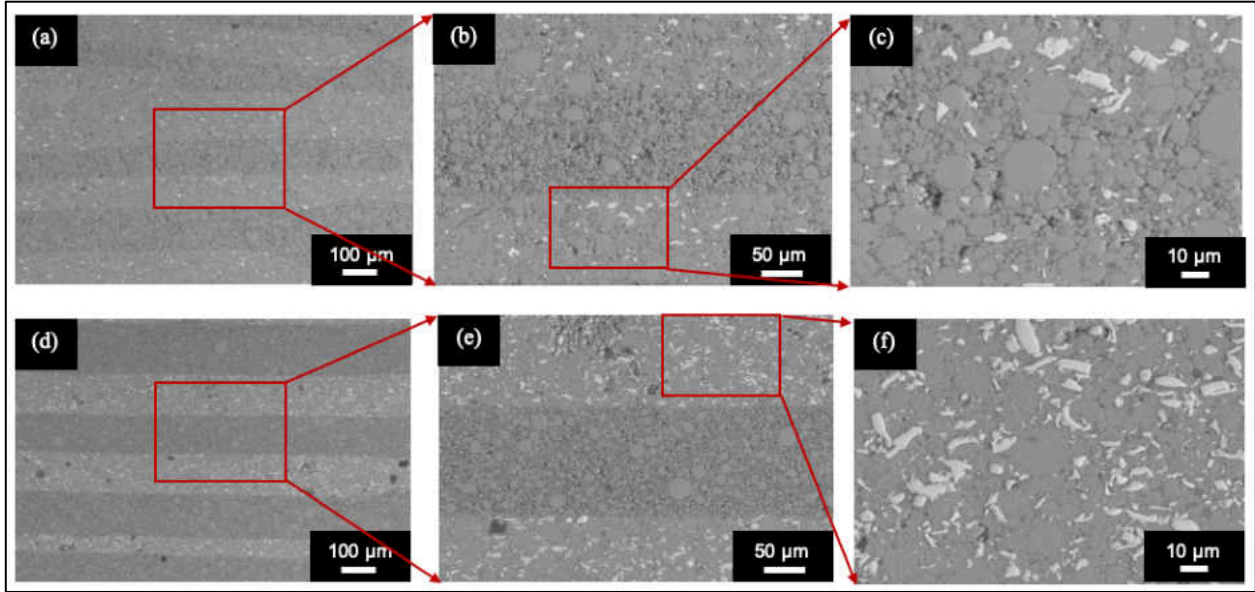
Figure 3.2: BSE SEM micrographs of, (a) AlSi-5%Ti$_3$SiC$_2$/AlSi, (b) higher magnification of the marked region (a), (c) microstructure of the AlSi-5%Ti$_3$SiC$_2$ laminate, (d) AlSi-20%Ti$_3$SiC$_2$/AlSi, (e) higher magnification of the marked region in (d), and (f) microstructure of the AlSi-20%Ti$_3$SiC$_2$ laminate.
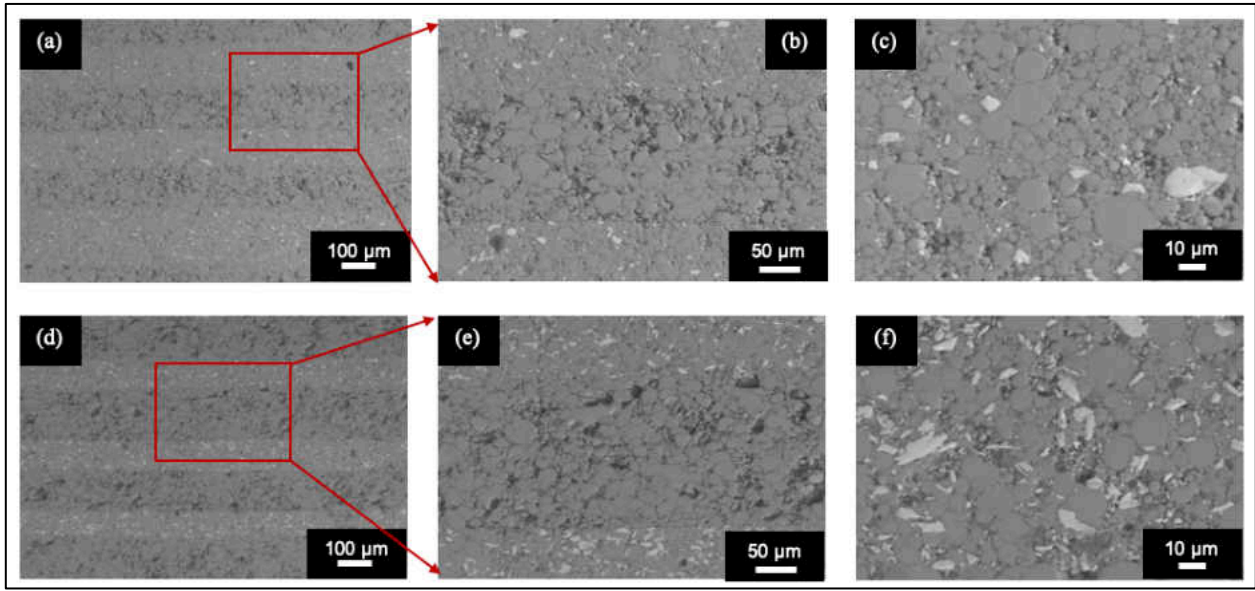
Figure 3.3: BSE SEM micrographs of, (a) AlSi-5%Ti$_3$SiC$_2$/Al, (b) higher magnification of the marked region in (a), (c) higher magnification of AlSi-5%Ti$_3$SiC$_2$ layer, (d) AlSi-20%Ti$_3$SiC$_2$/Al, (e) higher magnification of the marked region in (d), and (f) higher magnification of AlSi-20%Ti$_3$SiC$_2$ layer.

3.3.2 Mechanical Performance

Figure 3.4 plots the porosity and hardness of the composites as a function of Ti_3SiC_2 content. In all the samples, due to the lower formability temperature of AlSi matrix, the increase in Ti_3SiC_2 content did not had a remarkable effect on the porosity in the composite as compared to the multilayered Ni-matrix composites discussed in the last Chapter. In general, the hardness is decreased as the Ti_3SiC_2 content is increased in the parallel direction, however, the hardness is increased as the Ti_3SiC_2 content is increased in the perpendicular orientation (Fig. 3.4). It is hypothesized that due to post processing of the composites, it is difficult to accurately determine the location of the tested layers (for example, whether it is AlSi or AlSi-Ti_3SiC_2) in the parallel direction thus the overall hardness of the matrix decreased as the content of Ti_3SiC_2 was increased in the composites as compared to the perpendicular direction where the hardness was determined by the combination of all the layers.
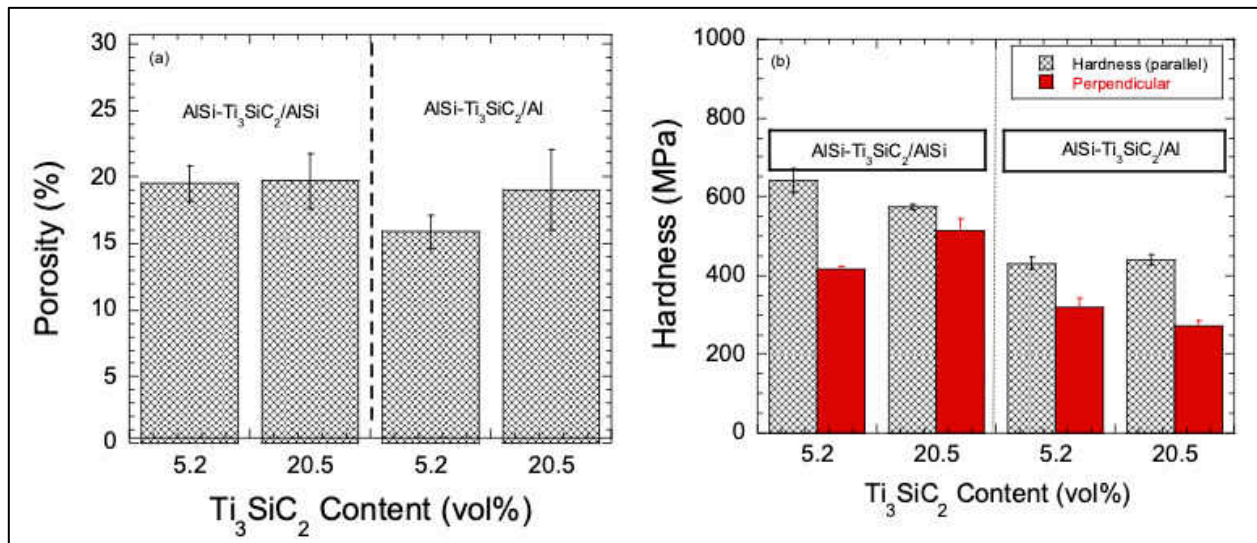
Figure 3.4 Plot of, (a) porosity, and (b) hardness in AlSi-Ti_3SiC_2/AlSi and Al- Ti_3SiC_2/Al multilayered composites as function of Ti_3SiC_2 content.

Figure 3.5 shows the stress versus displacement plots for the two tested composites. In all the plots, the failure in both direction happened in a similar manner. In the AlSi-Ti$_3$SiC$_2$ / AlSi composites (Fig. 3.6), the compressive strength increased as the Ti$_3$SiC$_2$ concentration was increased in the both direction. However, in the AlSi-Ti$_3$SiC$_2$ / Al composites, the UCS in the parallel direction remained the same whereas in the perpendicular direction the samples showed a decrease in compressive strength (Fig. 3.6). This study clearly proves that the addition of Ti$_3$SiC$_2$ particulates improves the hardness and yield strength of AlSi-Ti$_3$SiC$_2$/AlSi composites as compared to AlSi-Ti$_3$SiC$_2$/Al composites which shows that AlSi is more effective in forming a strong interface between AlSi-Ti$_3$SiC$_2$ composites as compared to Al.
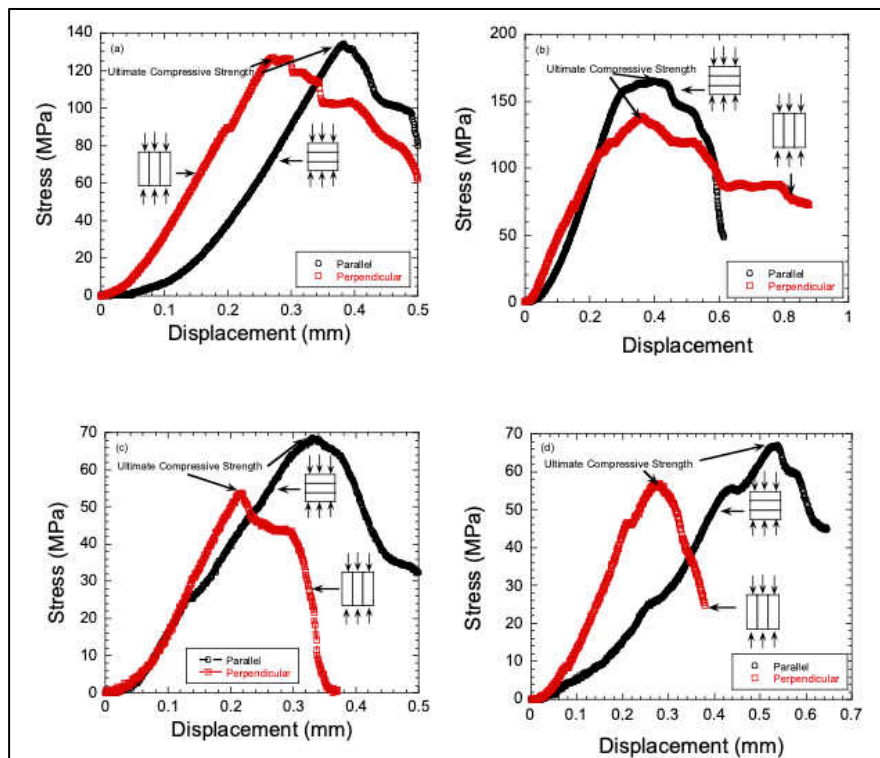
Figure 3.5 Plot of compressive stress versus displacement of, (a) AlSi-5%Ti$_3$SiC$_2$/AlSi, (b) AlSi-20%Ti$_3$SiC$_2$/AlSi, (c) AlSi-5%Ti$_3$SiC$_2$/Al, and (d) AlSi-20%Ti$_3$SiC$_2$/Al multilayered composites.
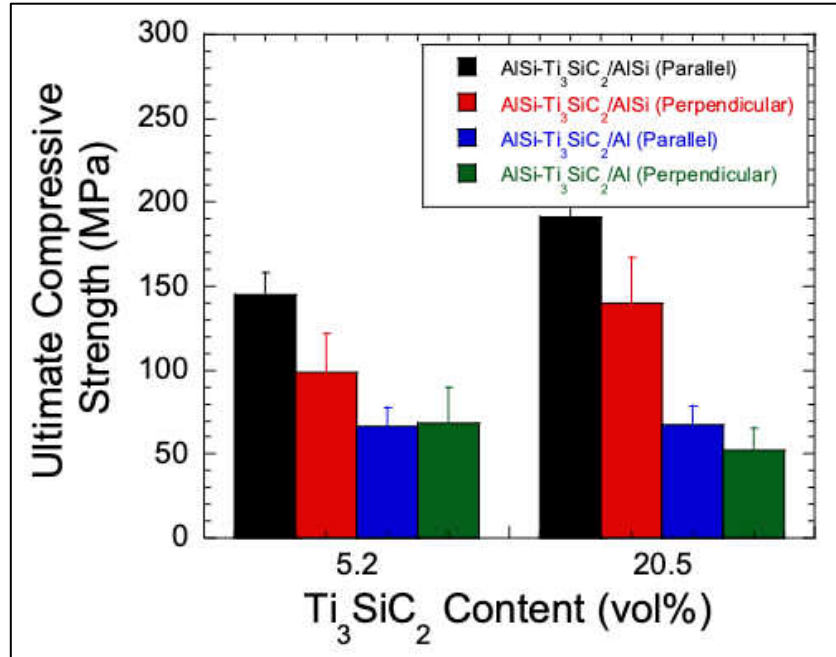
Figure 3.6 Plot of UCS versus Ti_3SiC_2 content in AlSi- Ti_3SiC_2/AlSi and AlSi- Ti_3SiC_2/Al multilayered composites

3.3.3 Tribological Behavior of AlSi-Ti$_3$SiC$_2$ / AlSi and Al Composites

Figures 3.6 a-b show the plot of WR and μ_{mean} of AlSi-Ti_3SiC_2/AlSi and AlS-Ti_3SiC_2/Al multilayered composites. In general, the WR decreased as the concentration of Ti_3SiC_2 increased (Fig. 3.6 a). In addition, WRs are significantly higher than the isotropic AlSi-Ti_3SiC_2 composite (please check Ref. 9 in Chapter 2 of this thesis for detailed manufacturing methods of isotropic samples) with the same Ti_3SiC_2 contents due to the presence of higher porosity in the multilayered composites. Currently, our team is designing isotropic samples with similar porosity for a more direct comparison. Figure 3.6 b shows the plot of μ_{mean} versus distance of AlSi-Ti_3SiC_2 / AlSi and AlSi-Ti_3SiC_2 / Al composites. The μ_{mean} decreased as the concentration of Ti_3SiC_2 was increased in the AlSi-matrix. It is important to note that despite the higher porosity, the multilayered AlSi-Ti_3SiC_2 composite had lower friction coefficient than the isotropic composites. We are further exploring these composites to understand the tribological behavior in detail.
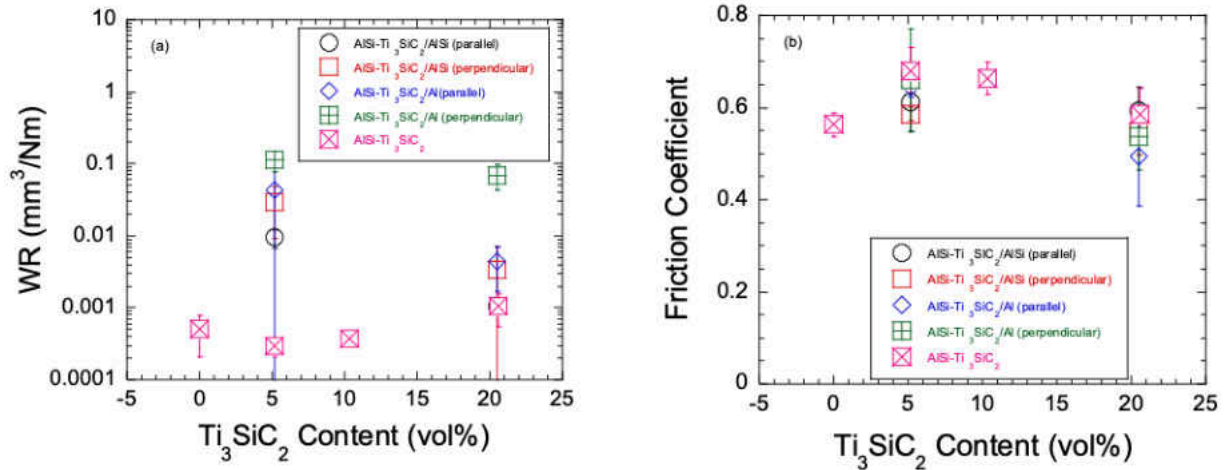
Figure 3.7: Plot of, (a) WR, and (b) μ_{mean} of AlSi-Ti$_3$SiC$_2$/AlSi and AlSi-Ti$_3$SiC$_2$/Al multilayered composites (data for isotropic AlSi-Ti$_3$SiC$_2$ samples are from Ref. 9 in Chapter 2 of this thesis).

3.4 Conclusions

In this study, AlSi- Ti$_3$SiC$_2$ / AlSi and AlSi-Ti$_3$SiC$_2$ / Al multilayered composites were synthesized for the first time. The microstructure evaluation by SEM (Scanning Electron Microscopy) showed that Ti$_3$SiC$_2$ particles are well dispersed in the AlSi matrix. The mechanical strength and tribological study showed promising results. We are investigating isotropic AlSi-Ti$_3$SiC$_2$ composites with similar porosity for a direct comparison.

CHAPTER IV

FUTURE STUDIES

During these studies, we investigated Ti_3SiC_2 as the particulate phase in designing multilayered MRMs. An important conclusion of this study was the direct correlation between layer thickness and UCS. Based on these facts, it is recommended that further research should focus on different types of MAX phases, and further properties should be investigated by varying layer thickness, MAX phases concentration, and metal matrix composition.

<div align="center">**APPENDIX**</div>

PRESENTATION DURING MASTER'S STUDY

"Design of Novel Ni-Ti$_3$SiC$_2$ based Multilayered Composites", Q. Tran, M. Fuka, M. Dey, and S. Gupta, "Proceedings of 42nd International Conference & Expo on Advanced Ceramics & Composites" (ICACC 2018).

STATUS OF JOURNAL PUBLICATIONS

"Synthesis and Characterization of Novel AlSi-Ti$_3$SiC$_2$ Multilayered Composites", Q. Tran, M. Dey, and S. Gupta, AIAA Propulsion & Energy Forum Proceedings, 2019 (submitted).

REFERENCE

CHAPTER I

[1] B. J. Hamrock, "Fundamentals of Fluid Film Lubrication", NASA reference publication 1255, pp 2, 1991.

[2] W. Shizhu, H. Ping, "Principles of Tribology", John Wiley & Sons, 2012.

[3] M. Fuka, MS Thesis, University of North Dakota (2018).

[4] W. Gross, etc., "Fluid Film Lubricating", John Wiley & Sons, 66, 718, 1980

[5] T. Sunil, M. Sandeep, R. Kumaraswami, A. Shravan, "A Critical Review on Solid Lubricants", IJMET, Vol. 7, Issue 5, 193-199, 2016.

[6] F. Clauss, "Solid Lubricants and Self-Lubricating Solids", 1st Ed. Academic Press, Inc., chapter 22.1 (1972)

[7] J. C. J. Bart, E. Gucciardi, S. Cavallaro, "Lubricants: Properties and Characteristics", Biolubricants, Science and Technology, Woodhead Publishing Series in Energy, 24-73, 2013

[8] S. Gupta, T. Hammann, R. Johnson, and M.F. Riyad, "Synthesis and Characterization of Novel Al-Matrix Composites Reinforced with Ti$_3$SiC$_2$ Particulates", Journal of Materials Engineering and Performance, 24, 1011-1017 (2014).

[9] T. Hammann, R. Johnson, M. F. Riyad, and S. Gupta, "Novel Ti$_3$SiC$_2$ reinforced Sn matrix composites", Proceedings of 39th International Conference & Expo on Advanced Ceramics & Composites (ICACC 2015).

[10] S. Gupta, M.A. Habib, R. Dunnigan, et al., "Synthesis and Characterization of Ti_3SiC_2 Particulate-Reinforced Novel Zn Matrix Composites", J. of Materi Eng and Perform, 24, 4071-4076 (2015).

[11] S. Gupta, F. AlAnazi, S. Ghosh, R. Dunnigan, "Synthesis and Tribological Behavior of Novel Ag- and Bi- Based Composites Reinforced with Ti_3SiC_2", Wear, 376, 1074-1083 (2017).

[12] M.W. Barsoum, T. El-Raghy, "The MAX Phases: Unique New Carbide and Nitride Materials: Ternary Ceramics Turn Out To Be Surprisingly Soft and Machinable, Yet Also Heat-Tolerant, Strong and Lightweight", American Scientist 89, 4, 334-343, (2001)

[13] M.W. Barsoum, "MAX Phases: Properties of Machinable Ternary Carbides and Nitrides", 1st ed. Wiley-VCH, 2013

[14] P. Eklund, M. Beckers, U. Jansson, H. Hogberg, L. Hultman, "The $M_{n+1}AX_n$ phases: Materials Science and thin-film processing", Thin Solid Films 518, 1851-1878 (2010)

[15] M.W. Barsoum, "The $M_{n+1}AX_n$ Phases: A New Class of Solids; Thermodynamically Stable Nanolaminates", Prog. Solid St. Chem, Vol 28, pp 201-281 (2000)

[16] M.W. Barsou, M. Radovic, "Elastic and Mechanical Properties of the MAX Phases", Annu. Rev. Mater. Res. 41, 195-227 (2011)

[17] U.S. Congress, Office of Technology Assessment, Advanced Materials by Design, OTA- E-351,Washington, DC: U.S. Government Printing Office, June 1988.

[18] M. Dey, M. Fuka, F. AlAnazi, S. Gupta, "Synthesis and Characterization of Novel Ni-Ti3SiC2 Composites", 42nd Int'l Conf. & Expo on Advanced Ceramic & Composites (ICACC), 2018

[19] M. Fuka, M. Dey, S. Gupta, "Novel Ternary Boride (MoAlB) Particulates as Solid Lubricant Additives in Ni-Matrix Composites", Joint Propulsion Conference, AIAA, 2018

[20] M.W. Barsoum, T. El-Raghy, "Synthesis and Characterization of a Remarkable Ceramic: Ti_3SiC_2", Journal of American Ceramic Society 79, 1953-1956 (1996)

[21] S. Gupta, "Tribology of MAX phases and their composites", PhD thesis, Drexel University, 2006

[22] S. Gupta, T. Hammann, R. Johnson, M.F. Riyad, "Tribological Behavior of Novel Ti_3SiC_2 (Natural Nanolaminates)-Reinforced Epoxy Composites during Dry Sliding", Tribology Transactions, 58, 560–566 (2015).

[23] S. Gupta, S. Ghosh, and R. Dunnigan, "Synthesis and Tribological Behavior of Novel Wear Resistant PEEK- Ti_3SiC_2 composites", Journal of Engineering Tribology, 231, 422-428 (2017).

[24] S. Ghosh, R. Dunnigan, M.A. Habib, and S. Gupta, "Novel MAX-Polymer Multifunctional Composites", Proceedings of 40th International Conference & Expo on Advanced Ceramics & Composites (ICACC 2016).

[25] V. Dolique, M. Jaouen, T. Cabioc'h, F. Pailloux, Ph. Guerin, V. Pelosin, "Formation of (Ti, Al)N/Ti_2AlN multilayers after annealing of TiN/TiAl(N) multilayers deposited by ion beam sputtering", Journal of Applied Physics 103, 2008.

[26] R. Grieseler, T. Kups, M. Wilke, M. Hopfeld, P. Schaaf, " Formation of Ti_2AlN nanolaminate films by multilayer-deposition and subsequent rapid thermal annealing", Material Letters 82, 74-77, 2012.

[27] A. Murugaiah, etc., "Tape Casting, Pressureless Sintering, and Grain Growth in Ti_3SiC_2 Compacts", Journal of American Ceramic Society, 87 [4], 550-560, 2004.

[28] C. Hu, Y. Sakka, H. Tanaka, T. Nishimura, S. Grasso, "Fabrication of Textured Nb_4AlC_3 Ceramic by Slip Casting in a Strong Magnetic Field and Spark Plasma Sintering", Journal of American Ceramic Society, 94 [2], 410-415, 2011.

CHAPTER II

[1] M. Jabbari, etc, "Ceramic Tape Casting: A Review of Current Methods and Trends with Emphasis on Rheological Behavior and Flow Analysis", Materials Science and Engineering B 212, 39-61, 2016

[2] S. Baklouti, J. Bouaziz, T. Chartier, J-F. Baumard, "Binder Burnout and Evolution of the Mechanical Strength of Dry-Pressed Ceramics Containing Poly(Vinyl Alcohol), Journal of the European Ceramic Society 21, 1087-1092, 2001

[3] S. Gupta, T. Hammann, R. Johnson, and M.F. Riyad, "Synthesis and Characterization of Novel Al-Matrix Composites Reinforced with Ti_3SiC_2 Particulates", Journal of Materials Engineering and Performance, 24, 1011-1017 (2014).

[4] T. Hammann, R. Johnson, M. F. Riyad, and S. Gupta, "Novel Ti_3SiC_2 reinforced Sn matrix composites", Proceedings of 39th International Conference & Expo on Advanced Ceramics & Composites (ICACC 2015).

[5] S. Gupta, M.A. Habib, R. Dunnigan, et al., "Synthesis and Characterization of Ti_3SiC_2 Particulate-Reinforced Novel Zn Matrix Composites", J. of Materi Eng and Perform, 24, 4071-4076 (2015).

[6] S. Gupta, F. AlAnazi, S. Ghosh, R. Dunnigan, "Synthesis and Tribological Behavior of Novel Ag- and Bi- Based Composites Reinforced with Ti_3SiC_2", Wear, 376, 1074-1083 (2017).

[7] T. Hammann, R. Johnson, M. F. Riyad, and S. Gupta, "Effect of Ti_3SiC_2 Particulates on the Mechanical and Tribological Behaviors of Sn-Matrix Composites", Proceedings of 39th Int'l Composite & Expo on Advanced Ceramics & Composites (ICACC 2015).

[8] M. Fuka, MS Thesis, University of North Dakota (2018).

[9] M. Dey, MS Thesis, University of North Dakota (2018).

CHAPTER III

[1] N. Mahallawy, A. Fathy, A. Abdelaziem, M. Hassan, "Microstructure evolution and mechanical properties of Al/Al-12%Si multilayer processed by accumulative roll bonding (ARB)", Material Science & Engineering A 647, 127-135, 2015.

[2] N. Mahallawy, A. Fathy, M. Hassan, "Evaluation of mechanical properties and microstructure of Al/Al-12%Si multilayer via warm accumulative roll bonding process", Journal of Composite Materials, 1-11, 2017

[3] Y. Birol, "Microstructural Evolution During Annealing of a Rapidly Solidified Al-12%Si Alloy", Journal of Alloys and Compounds 439, 81-86, 2007